RSC Advances

PAPER

View Article Online
View Journal | View Issue



Cite this: *RSC Adv.*, 2020, **10**, 15072

# $CO_2$ conversion into methanol under ambient conditions using efficient nanocomposite photocatalyst/solar-energy materials in aqueous medium†

Mohsen Lashgari *[ab] and Sanaz Soodi[a]

A promising route to solve the $CO_2$ issue is its photocatalytic back-conversion to H-based solar fuels/chemicals, particularly methanol – being widely used as a strategic material in chemical/energy-related industries. Herein, the authors address this globally interesting problem and demonstrate how through an effortless hydrothermal route and using earth-abundant elements, two efficient carbon nanotube (CNT)-based heterojunction photocatalyst/solar-energy materials, *viz.* CNT/NiO and CNT/NiO/$Fe_2O_3$ are synthesized and employed for methanol production. The investigations revealed that both binary and ternary composites could selectively (≥93%) produce methanol using $CO_2$ feed in aqueous medium. Moreover, a higher performance (energy efficiency: 1.81%) was witnessed for the ternary photocatalyst. From a catalytic standpoint, the superior activity of the CNT/NiO/$Fe_2O_3$ photocatalyst was discussed in detail in terms of its larger surface area, higher absorption of incident light, better charge separation/transfer, and generation of greater photo-voltage/current to effectually split the water medium and achieve the photoconversion process. A mechanistic scheme was finally proposed for the production of methanol and methane, as liquid and gas phase products, respectively.

Received 23rd February 2020
Accepted 2nd April 2020

DOI: 10.1039/d0ra01733g

rsc.li/rsc-advances



## Introduction

Methanol ($CH_3OH$) is a strategic chemical with wide application in the synthesis of hydrocarbons, plastics, pharmaceuticals, adhesives and so forth. This compound is also important from an energy perspective and is considered a safe H-based fuel – that is employed in direct methanol fuel cells or utilized as a blend with gasoline in internal combustion engines.[1,2]

Current technologies to synthesize methanol are mainly based on production and consumption of syngas mixture [the output of steam reforming process], being industrially carried out under harsh high temperature/pressure conditions ($T$ = 200–300 °C, $P$ = 5–10 MPa) through catalytic hydrogenation of a $CO_2$/CO feed:[2,3]

$$\begin{aligned} CO + 2H_2 &\rightarrow CH_3OH \\ CO_2 + 3H_2 &\rightarrow CH_3OH + H_2O \end{aligned} \quad (1)$$

During the hydrogenation process, $H_2$ molecules are dissociated upon the catalyst surface and the resulting H atoms are combined with $CO_2$/CO molecules and transformed into methanol. Although methanol can be synthesized by either CO or $CO_2$ feed, the use of $CO_2$ is preferred from non-toxicity standpoint.[4,5]

Carbon dioxide transformation [back-conversion] into methanol is also crucial from the environmental viewpoint,[1] since this notorious greenhouse gas – being unrestrictedly produced by human societies and dumped into the atmosphere – is universally deemed the main cause of global warming and climate change.[6] Therefore, this plentiful ubiquitous gas can be reconsidered a sustainable complimentary source of carbon and be utilized in the synthesis of other C-based chemicals/fuels,[7,8] particularly methanol as pointed above.

Artificial photosynthesis of methanol using $CO_2$ upon semiconductor materials in aqueous medium, is a modern/green strategy,[9] in which H atoms (radicals) are transiently generated on the photocatalyst surface ($H^+ + e_{cb}^- \rightarrow H$[10]) and subsequently utilized in $CO_2$ conversion (hydrogenation) to methanol.

One of the challenging issues in the photocatalytic back-conversion of $CO_2$ into oxygenates is selective synthesis of a specific compound and reduction of the diversity of by-products.[7,11] This objective can be met by proper selection of photocatalyst components.[12] In the present work, we chose NiO semiconducting component, owing to nickel property in $CO_2$ adsorption and its capability to produce methanol.[4,13,14] We also

[a]*Chem. Dept, Institute for Advanced Studies in Basic Sciences (IASBS), 444 Prof. Yousef Sobouti Blvd., Zanjan 45137-66731, Iran. E-mail: Lashgari@iasbs.ac.ir*

[b]*Center for Research in Climate Change and Global Warming: Hydrogen and Solar Division, Zanjan 45137-66731, Iran*

† Electronic supplementary information (ESI) available. See DOI: 10.1039/d0ra01733g

employed carbon nanotube (CNT), because it has been reported as an effective component for photocatalytic conversion of $CO_2$ into solar fuels, particularly alcohols.[9,15,16] Furthermore, it is worth noting that CNT has the capacity of hydrogen storage.[17] Therefore, on the resulting CNT/NiO composite material, the hydrogenation of $CO_2$ could occur effectively, and an appreciable amount of methanol is anticipated to be produced upon this binary nanocomposite photocatalyst.

Since NiO is a wide-bandgap, p-type semiconducting material, a straightforward strategy to improve its photon absorption and reduce charge (e/h) recombination phenomenon, is to make its composite with a suitable low-cost, eco-friendly, narrow-bandgap, n-type semiconductor, *viz.* $Fe_2O_3$.[8,18–20] Based on this strategy, herein, we also synthesized a ternary CNT/NiO/$Fe_2O_3$ composite as an efficient photocatalyst/solar-energy material for application in $CO_2$ transformation into methanol. Concerning the photocatalytic application of NiO/$Fe_2O_3$, it should be finally noted that these semiconducting components have been also employed in the literature, for water oxidation and dye (pollutant) degradation as well.[18,19,21,22]

The objective of this research is to reduce the diversity of products and perform selective photosynthesis of methanol by means of proper selection of photocatalyst components and their synthesis through a facile hydrothermal route using earth abundant elements. To better understanding of the photocatalyst activity, besides geometrical/morphological as well as photochemical factors, we will also pay particular attention on photoelectrochemical concepts, including photovoltage and photocurrent as two new thermodynamic and kinetic parameters influencing on the activity of photocatalysts. Another interesting feature of this article is its mechanistic interpretation of the photosynthesis phenomenon.

# Experimental

### Photocatalyst synthesis

The binary and ternary composite energy-materials, *i.e.* CNT/NiO and CNT/NiO/$Fe_2O_3$ were hydrothermally synthesized according to the literature with some modifications.[23–26] Prior to the synthesis of photocatalysts, CNT (multiwall, purchased from Neutrino CNT-manufacturing company; internal and external diameters 3 and 6.3 nm, respectively[17]) was thoroughly washed and dispersed using a sonication bath in acetone (30 min), ethanol (1 h), and deionized water (DW, 30 min) and finally dried in a vacuum desiccator overnight at room temperature. To synthesize CNT/NiO, an appropriate quantity of the purified CNT [3 wt%; Fig. S1†] was ultrasonically dispersed in a 30 ml DW/ethanol (1 : 1 v/v) solution containing 0.12 M $Ni^{2+}$ ($NiCl_2 \cdot 6H_2O$ salt, Sigma-Aldrich; 99%), 0.07 M hexamethylenetetramine ($C_6H_{12}N_4$, Merck; 99%), and 2 ml ethanolamine ($NH_2(CH_2)_2OH$, Merck; 98%). The suspension was then transferred into a Teflon-lined stainless steel autoclave and heated for a day at 160 °C. After cooling the reactor, the reaction mixture was decanted, washed several times with ethanol and DW, and dried at 60 °C. Finally, the resulting compound was heated (5 °C $min^{-1}$) under argon atmosphere, and stayed at 350 °C for 1 h.

To synthesize CNT/NiO/$Fe_2O_3$, 10 mg of the freshly prepared CNT/NiO powder was added to 16 ml DW containing 0.032 M sodium sulfate salt ($Na_2SO_4 \cdot 10H_2O$, Sigma-Aldrich; 98%). Under vigorous stirring of the mixture, an optimum quantity of $Fe^{3+}$ cation [2 : 1 $Fe^{3+}$ to $Ni^{2+}$ molar ratio; see Fig. S1†], *i.e.* 240 mmol ferric nitrate ($Fe(NO_3)_3 \cdot 9H_2O$ salt, Sigma-Aldrich; 98%) was dissolved in the mentioned medium. The resulting mixture was then transferred into the autoclave reactor and heated for 2 h at 120 °C. After cooling the reactor, the precipitate was similarly washed several times with ethanol and DW, dried at 80 °C and finally calcined at 400 °C under argon atmosphere for 2 h (heating rate: 5 °C $min^{-1}$).

### Characterization (XRD, XPS, Raman, SEM, BET, DR, PL, and photoelectrochemical analyses)

X-ray diffraction (XRD) patterns of the synthesized materials were determined using a Philips X'Pert Pro X-ray powder diffractometer ($\lambda = 1.54$ Å; Cu-K$\alpha$ beam). XPS spectra were recorded *via* a Thermo Scientific™ ESCALAB™ 250Xi photoelectron spectrometer with Mg-K$\alpha$ X-ray source (1253.6 eV). Raman spectra were recorded at room temperature using a Rigaku FirstGuard hand-held spectrometer with a 1064 nm laser and TE (Thermoelectric) Cooled CCD (Charge Coupled Device) detector. Field emission scanning electron micrographs (FE-SEM) of the synthesized materials were taken using a Tescan Mira3 electron microscope. Nitrogen adsorption–desorption (BET) and porosimetry tests were conducted at 76 K on a Micromeritics® TriStar II Plus analyzer. Diffuse reflectance (DR) spectra of the photocatalysts were measured using a Varian Cary 5 UV-Vis-NIR spectrometer ($BaSO_4$ was used as a blank). To record photoluminescence (PL) spectra of the photocatalyst materials, a Varian Cary Eclipse fluorescence spectrophotometer was utilized ($\lambda_{ex} = 409$ nm).

Open circuit potential (OCP), transient photocurrent and impedance measurements of the photocatalyst powders were conducted in a conventional 3-electrode glass cell using an Ivium-Vertex Potentio-Galvanostat instrument (electrolyte: a 0.5 M $NaHCO_3$ solution, light source: a 10 W blue LED with $\lambda = 434$ nm).[7,17] In these tests, a platinum foil (2.5 $cm^2$) and saturated calomel (SCE) were employed as counter and reference electrodes, respectively. The working electrodes (WEs) were also fabricated through a Dr Blade approach[27] by mixing 20 mg photocatalyst, 3 drops Triton X-100 (surfactant, serving as binder) and 0.25 ml DW, and coating the resulting paste on the conductive side of a 1 × 1 $cm^2$ fluorine doped tin oxide (FTO) glass (SOLARONIX, electrical resistance: 10 Ω $sq^{-1}$). Then, the electrodes were dried at 60 °C for 15 min and finally annealed at 250 °C for 60 min. By applying a small potential bias to WE (~10 mV w.r.t. OCP), the transient photocurrent tests were carried out under a situation, where the background (dark) current was almost zero and its sign was not changed during the light-on/off cycles [OCPs for CNT/NiO and CNT/NiO/$Fe_2O_3$ were ~295 and 287 $mV_{SCE}$, respectively].

### Photocatalytic conversion of $CO_2$ into methanol: photoreactor setup and product analysis

The photoconversion/hydrogenation process was conducted in an upright, cylindrical, double-wall, glass reactor attached to a T-controlling bath circulator (WCR-P6). The reaction medium

was 50 ml DW containing 50 mg suspended photocatalyst and dissolved $CO_2$ gas. To increase the solubility of the gas as well as improve the photocatalyst performance, the pH of medium was set at 8.5 using a NaOH solution.[7,28] Prior to illumination of the reactor, the medium was saturated with a pure 99.99% $CO_2$ gas (under saturated condition, the pH of medium reaches ~7.5 and bicarbonate is the predominant species in the medium[29,30]). During the test, the photocatalyst particles were continuously dispersed using a magnetic stirrer, and the bubbling of $CO_2$ gas into the reaction medium continued in a smooth flow (~40 ml $min^{-1}$). A sun simulated light (xenon irradiation, 100 mW $cm^{-2}$)[17] was employed and the tests were terminated after 2 h illumination of the reactor (according to our previous reports, the illumination at longer periods is not recommended for the studies of liquid-phase products, because by accumulating the product in the reaction medium, it can undergo further reaction/degradation and becomes consequently consumed[7,9]).

The water photo-splitting experiment was conducted in the same photoreactor (containing 50 ml DW and 50 mg photocatalyst powder) in the absence of any additive, and the volume of photogenerated gas was recorded at different illumination periods in a route described in detail elsewhere.[31,32]

The quantity of methanol and other by-products in the aqueous reaction medium was determined using a high performance liquid chromatographic (HPLC) approach.[33,34] To this end, a Knauer HPLC instrument equipped with UV and RI detectors (K2600, K2310) and a Eurokat H column (300 × 8 mm, 10 μm) was applied [eluent: 0.05 M $H_2SO_4$, temp: 60 °C, flow rate: 0.6 ml $min^{-1}$]. All measurements were repeated at least three times and the mean values were reported as final data.

## Results and discussion

### Photocatalyst synthesis and characterization

X-ray diffraction (XRD) patterns of the binary (CNT/NiO) and ternary (CNT/NiO/$Fe_2O_3$) nanocomposites are depicted in Fig. 1.

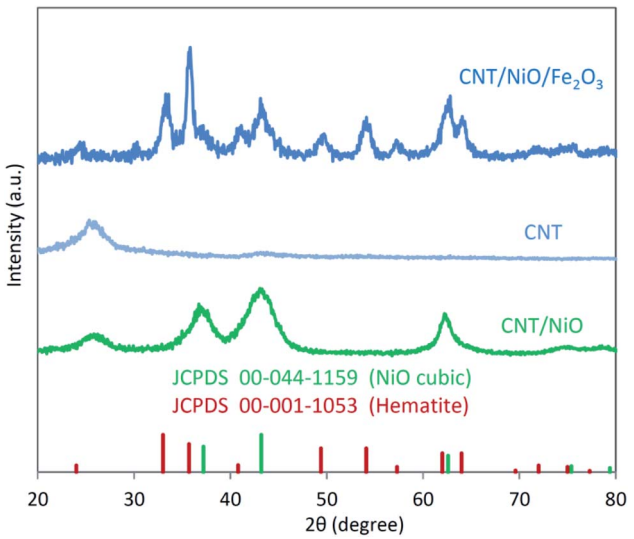


Fig. 1 X-ray diffraction (XRD) patterns of the binary and ternary CNT-based photocatalyst/solar-energy materials synthesized in this work.

Table 1 XPS results for the composite photocatalyst containing all components

| Atom | Spectral line | Binding energy (eV) | Assigned to | Reference |
|---|---|---|---|---|
| C | 1s | 284.6 | CNT | 35 |
| Fe | $2p_{1/2}$ | 724.0 | $Fe_2O_3$ | 10, 33 and 34 |
| | $2p_{3/2}$ | 710.4 | | |
| Ni | $2p_{1/2}$ | 873.1 | NiO | 34 |
| | $2p_{3/2}$ | 854.6 | | |
| O | 1s | 530.1 | $Fe_2O_3$, NiO | 34 |

Similar to our previous reports, the existence of CNT in these composite materials is recognized as a relatively wide, low-intensity peak between 20 to 30 degrees.[8,33] By comparing the

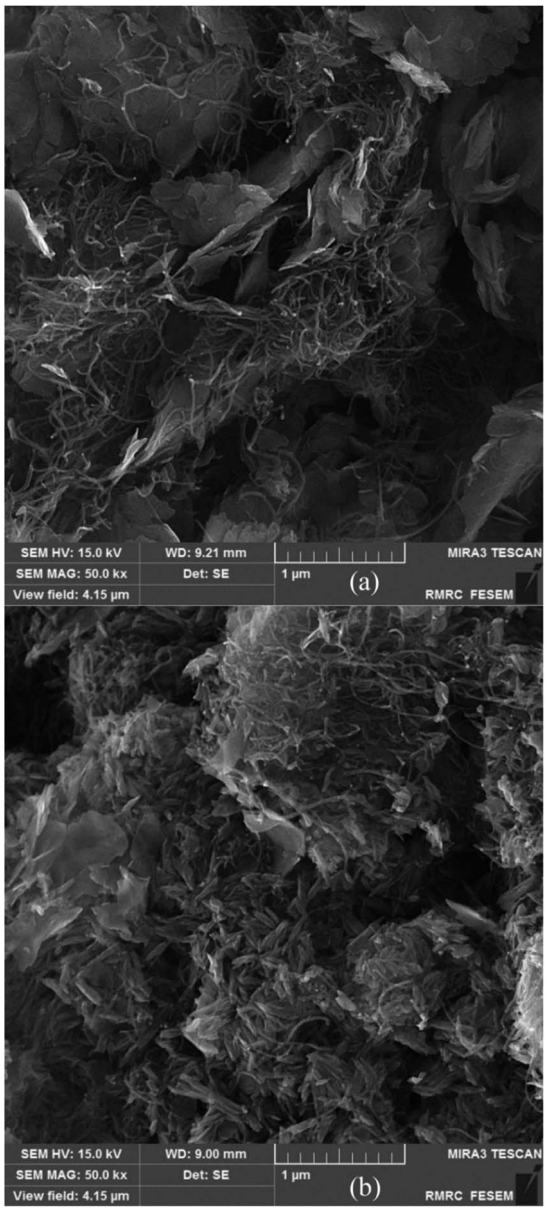


Fig. 2 SEM images of CNT/NiO (a) and CNT/NiO/$Fe_2O_3$ (b) nanocomposite materials under consideration.

XRD pattern of CNT/NiO with that of NiO (JCPDS card no. 00-044-1159), the formation of the binary composite is clearly affirmed. Furthermore, the occurrence of wide peaks in XRD diagrams indirectly indicates that the energy materials synthesized here have nanostructured morphology.[9,31] Fig. 1 also shows that compared to the XRD diagram of CNT/NiO, the ternary composite, *i.e.* CNT/NiO/$Fe_2O_3$ has a more complicated pattern, which is owing to the existence of $Fe_2O_3$ component (JCPDS card no. 44-1159) in this composite material. In addition to XRD, the presence of Ni, Fe, O, C and the formation of NiO, $Fe_2O_3$ and CNT were confirmed using XPS data (Table 1). The synthesis of NiO and $Fe_2O_3$ as well as the existence of CNT in the composite material were also approved by Raman evidence (Fig. S4†). The nanostructured morphology witnessed *via* XRD diagram (peak broadening; see Fig. 1) was confirmed by SEM images taken from both binary and ternary photocatalysts (Fig. 2). Fig. 2a shows a porous nano-flake/flower-like structure (the characteristic of NiO[23–25]) in which CNT fibers are distributed in a relatively uniform manner within the composite photocatalyst. Besides NiO nano-flakes and CNT fibers, in the SEM image of the ternary photocatalyst (Fig. 2b), the existence of $Fe_2O_3$ was recognized as rod-shaped entities (see also Fig. S5 and S6†). The porous morphology of the photocatalysts was approved through BET analyses (Table 2 and Fig. S7†); here, a mesoporous structure (pore diameter: ~12 nm) was obtained for both photocatalysts, and a larger surface area as well as more pore volume were found in the presence of $Fe_2O_3$ component.

## Optical/photo-electrochemical response and activity prediction

Fig. 3a shows that CNT/NiO has a fair photon absorption in the visible region. This interesting ability of the photocatalyst to absorb incident light is ascribed to the existence of CNT in the composite material[17] (Fig. S8†). By adding $Fe_2O_3$ to the binary composite, the extent of photon absorption increases and its bandgap decreases from 2.7 eV to 1.6 eV (see Fig. S10†). Fig. 3b displays lower PL emission for the CNT/NiO/$Fe_2O_3$ photocatalyst, indicating the existence of a greater opportunity for the photogenerated charges in this photocatalyst to be effectually consumed in the photoredox process, before they get naturally annihilated through the e/h recombination phenomenon.[36]

The better charge separation witnessed for the ternary composite was reconfirmed by photo-electrochemical studies (Fig. 4), as a producing a higher transient photocurrent and greater photo-voltage [shift in OCP due to system illumination]

Table 2 Surface area and porosimetry data of the composite photocatalysts, obtained from $N_2$ adsorption–desorption (BET) studies

| Photocatalyst | Surface area ($m^2\ g^{-1}$) | Total pore volume[a] ($cm^3\ g^{-1}$) | Pore diameter[a] (nm) |
|---|---|---|---|
| CNT/NiO | 124 | 0.37 | 12.1 |
| CNT/NiO/$Fe_2O_3$ | 141 | 0.41 | 11.8 |

[a] Mean value.

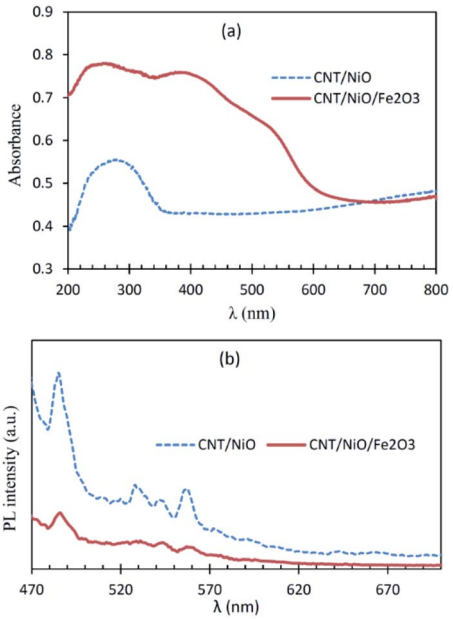


Fig. 3 Diffuse reflectance (DR) UV-Vis (a) and photoluminescence (PL; (b)) spectra of the nanocomposite photocatalyst/solar-energy materials under study.

as well as less electrical resistance (impedance) against charge transport.[37] Because of these reasons and the superior potency in harnessing the incident photons as well as possessing a larger surface area (Table 2), the ternary composite is anticipated to exhibit higher activity to convert $CO_2$ into methanol [see the next section].

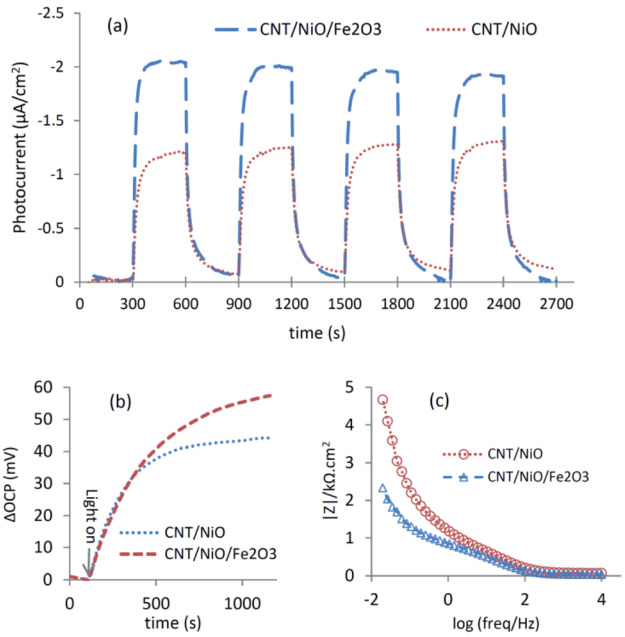


Fig. 4 Photoelectrochemical response of the nanocomposite photocatalysts: (a) transient photocurrent (300 s light-on, 300 s light-off), (b) OCP-shift under system illumination depicted *vs.* time, and (c) Bode plot (impedance diagram).

Table 3 Summary of the analysis of products in the reaction medium (liquid phase) measured after 2 h operation of the $CO_2$ photoconversion reactor

| Product (μM) | Methanol | Oxalic acid | Formic acid | Acetic acid |
|---|---|---|---|---|
| CNT/NiO | 1655.0 | 64.5 | 33.1 | Trace |
| | (94.4)[a] | (3.7) | (1.9) | — |
| | (0.68)[b] | (0.08) | (0.01) | — |
| CNT/NiO/$Fe_2O_3$ | 4382.0 | 179.2 | 114.3 | 41.7 |
| | (92.9)[a] | (3.8) | (2.4) | (0.9) |
| | (1.81)[b] | (0.24) | (0.05) | (0.02) |

[a,b] data listed in these parentheses (rows) denote respectively to the selectivity (%) and energy efficiency (%), obtained for the photoconversion process to produce a specific product upon the photocatalyst material.

### $CO_2$ photoreduction in aqueous medium, methanol synthesis, and mechanistic perspective

$CO_2$ photoreduction reaction in the aqueous medium was performed under ambient conditions in the presence of binary and ternary composites, and the results of products analysis are summarized in Table 3.

Table 3 indicates that methanol is the main product of the $CO_2$ photoreduction process; by adding $Fe_2O_3$ to the binary composite, the capability of photocatalyst to produce methanol increases significantly (~2.6 times). To determine the ability of photocatalysts in selective production of methanol [among the liquid phase products], the authors employed this formula:

$$S(\%) = \frac{C_{\text{methanol}}}{\sum C_i} \times 100 \quad (2)$$

where, $C_i$ denotes the concentration of product i in the reaction medium and the summation is running over all products. Data listed in Table 3 show that both composite photocatalysts under consideration can effectively transform $CO_2$ into methanol and their selectivity for methanol production is above 92%. The energy efficiency of the photoconversion process was determined using eqn (3):[9,37]

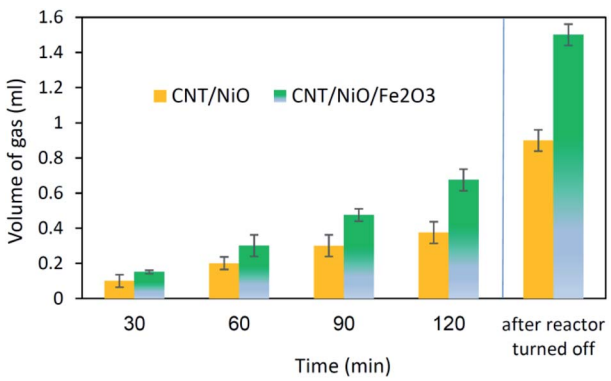


Fig. 5 The ability of photocatalysts to split water medium in the absence of any additive (sacrificial agent); the volume of the photogenerated gas was measured at different time intervals [reaction/illumination periods]. At the end of process, after 1 h from the photoreactor switched off, extra amount of gas was released.

$$\varepsilon(\%) = \frac{Qn}{\xi\tau} \times 100 \quad (3)$$

where, $Q$ is the heat of combustion, $n$ the mole of photosynthesized product and $\xi$ the power of incident light, and $\tau$ the reactor illumination period. In the present work, the maximum energy efficiency (1.81%) was obtained for the methanol production using the ternary photocatalyst.

Briefly, the superior activity of the ternary composite photocatalyst can be rationalized to its ability in: (1) possessing a larger surface area, (2) absorbing more incident photons, (3) exhibiting less charge (e/h) recombination, (4) facilitating charge transfer, and (5) producing more photo-voltage (photogenerated electromotive force). Furthermore, it should be noted that the ternary photocatalyst has greater potency in utilizing photogenerated charges ($h\nu \xrightarrow{SC} e_{cb}^- + h_{vb}^+$) to split water medium; see Fig. 5. The redox reactions occurring during the water-splitting process are proton reduction (eqn (4)) and hydroxide oxidation (eqn (5)), and the overall process is splitting of $H_2O$ molecules:[17,38]

$$\begin{array}{l} +\begin{cases} 2[H^+ + e^- \rightarrow H] \\ 2H \rightarrow H_2 \end{cases} \\ \hline 2H^+ + 2e^- \rightarrow H_2 \end{array} \quad (4)$$

$$\begin{array}{l} +\begin{cases} 2[OH^- + h^+ \rightarrow \dot{O}H] \\ 2\dot{O}H \rightarrow H_2O_2 \\ H_2O_2 \rightarrow H_2O + \frac{1}{2}O_2 \end{cases} \\ \hline 2OH^- + 2h^+ \rightarrow H_2O + \frac{1}{2}O_2 \end{array} \quad (5)$$

$$\begin{array}{l} +\begin{cases} 2H^+ + 2e^- \rightarrow H_2 \\ 2OH^- + 2h^+ \rightarrow H_2O + \frac{1}{2}O_2 \\ 2H_2O \rightleftharpoons 2H^+ + 2OH^- \end{cases} \\ \hline \therefore H_2O \rightarrow H_2 + \frac{1}{2}O_2 \end{array} \quad (6)$$

Concerning the capability of photocatalysts to split $H_2O$, Fig. 5 demonstrates that both composites are able to perform the water splitting process and the superior activity is due to CNT/NiO/$Fe_2O_3$. This evidence proposes the conjecture that during the water splitting process, not only more hydrogen but more hydroxyl could also be transiently generated upon the ternary photocatalyst surface.[10] With the generation of more H/OH radicals and facilitation of the hydrogenation of methoxyl or hydroxylation of methyl radicals (eqn (7)), the production of greater quantity of methanol (Fig. 6) is rationalized:[11,39–41]

$$\left.\begin{array}{c} \dot{C}H_3O + \dot{H} \\ \text{or} \\ \dot{C}H_3 + \dot{O}H \end{array}\right\} \rightarrow CH_3OH \quad (7)$$

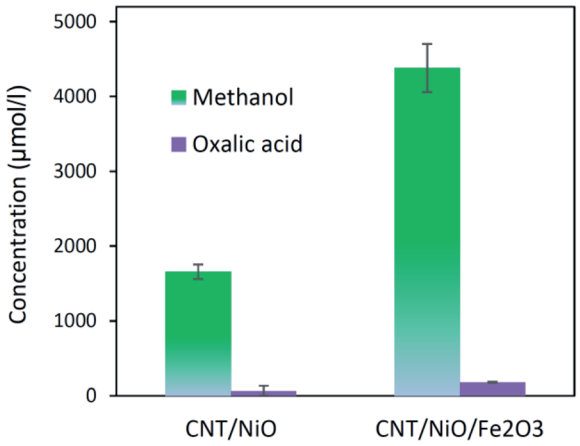


Fig. 6 The power of photocatalysts to convert $CO_2$ into methanol and oxalic acid (the main liquid-phase by-product).

In connection with this mechanistic route, it should also be noted that the transient generation of radical species mentioned above has been already witnessed elsewhere through EPR (electron paramagnetic resonance) and *in situ* FT-IR (Fourier transform infrared) spectroscopic techniques.[5,11,12,41–44]

The other point – deducing from eqn (7), is the possibility of $\dot{C}H_3 + \dot{H}$ recombination and hence the generation of methane as a gas-phase product. This anticipation was just verified for the ternary photocatalyst – that is able to produce extra methanol [see Fig. 6 and S12†]. Furthermore, it is worth noting that the non-production of methane upon the binary photocatalyst can be used to elucidate why less methanol becomes produced on CNT/NiO photocatalyst; here, the lack of methane formation ($C\dot{H} + \dot{H} \nrightarrow CH_4$) signifies that the available route for the methanol production is $CH_3\dot{O} + \dot{H}$ reaction not $\dot{C}H_3 + \dot{O}H$ alternative. By contrast, in the case of ternary photocatalyst, since methane is produced ($\dot{C}H_3 + \dot{H} \rightarrow CH_4$), both reaction channels (eqn (7)) are available; therefore, the production of more quantity of methanol is justified.

The final interesting fact that can be deduced from Fig. 5 is concerned with the H-sorbing capacity of CNT, justifying why by ending the reactor illumination, the gas evolution process is not immediately stopped. From photo-transformation standpoint, this property of the catalyst component is important, because CNT could indeed serve as an *in situ* H-reservoir system[13] for the hydrogenation of $CO_2$ on the photocatalyst surface.

## Conclusions

As a synopsis, in the present study, the authors focussed on the matter of selective photocatalytic transformation of $CO_2$ into methanol. To this end, two effective, eco-friendly, affordable CNT-based heterojunction nanocomposite photocatalysts were synthesized through a facile hydrothermal route. It was proved that both photocatalyst/solar-energy materials were able to selectively (≥93%) photosynthesize methanol. Since photocatalytic phenomena have an electrochemical nature, *i.e.* within them, a couple of redox (electron transport) reactions occur synchronously on the photocatalyst surface, these photo-induced phenomena could be electrochemically characterized *via* measuring the photogenerated voltage and current as two new determinant factors in the evaluation (justification) of the photocatalysts activity. Here, photovoltage (generated by striking photons onto the photocatalyst surface) plays a role of driving (electromotive) force for performing the redox reactions and photocurrent is the rate of electron transport, which could roughly represent a kinetic feature of the process. Besides points mentioned above, the following remarks were concluded:

❖ In the absence of any additive (sacrificial agent), both photocatalysts were able to split water molecules and serve as *in situ* H generator for $CO_2$ hydrogenation to methanol.

❖ With addition of $Fe_2O_3$ to the binary composite (CNT/NiO), not only the system impedance decreased, but its surface area as well as its potency to effectually harness incident photons were increased. Upon the resulting ternary photocatalyst (CNT/NiO/$Fe_2O_3$), a greater amount of methanol (more than twice) was produced.

❖ In the case of CNT/NiO/$Fe_2O_3$, by illuminating the reaction medium, a larger photo-voltage/current was generated and the splitting of water molecules as well as methanol production occurred in a superior extent.

❖ For methanol synthesis upon the ternary photocatalyst, both $\dot{C}H_3 + \dot{O}H$ and $CH_3\dot{O} + \dot{H}$ reaction channels were available and methane ($\dot{C}H_3 + \dot{H}$) was the main gas-phase product. Whereas in the case of binary photocatalyst, the reaction channel was limited to $CH_3\dot{O} + \dot{H}$ and no methane was produced.

## Conflicts of interest

There are no conflicts to declare.

## Acknowledgements

The authors wish to acknowledge the research council of IASBS for financial support of this project (GIASBS201932603). SS should thank Prof. Andreas Züttel for her hosting at EPFL and Lab facility for GC tests of gaseous products. We would also like to extend our thanks to the Editor as well as anonymous Referees of the manuscript for their efforts and useful comments.

## Notes and references

1 G. A. Olah, *Angew. Chem., Int. Ed.*, 2005, **44**, 2636.
2 S. G. Jadhav, P. D. Vaidya, B. M. Bhanage and J. B. Joshi, *Chem. Eng. Res. Des.*, 2014, **92**, 2557.
3 F. Studt, M. Behrens, E. L. Kunkes, N. Thomas, S. Zander, A. Tarasov, J. Schumann, E. Frei, J. B. Varley, F. Abild-Pedersen, J. K. Nørskov and R. Schlçgl, *ChemCatChem*, 2015, **7**, 1105.

4 F. Studt, I. Sharafutdinov, F. Abild-Pedersen, C. F. Elkjær, J. S. Hummelshøj, S. Dahl, I. Chorkendorff and J. K. Nørskov, *Nat. Chem.*, 2014, **6**, 320.
5 W. Wang, S. Wang, X. Ma and J. Gong, *Chem. Soc. Rev.*, 2011, **40**, 3703.
6 M. Lashgari, Use of solar and alternative energy to reduce emissions, *US-Iran Symposium on Climate Change: Impacts and Mitigation, March 30–April 1*, Irvine, California, 2015.
7 M. Lashgari and S. Soodi, *J. Nanosci. Nanotechnol.*, 2019, **19**, 3237.
8 Z. Yang, J. Xu, C. Wu, H. Jing, P. Li and H. Yin, *Appl. Catal., B*, 2014, **156–157**, 249.
9 M. Lashgari, S. Soodi and P. Zeinalkhani, *J. $CO_2$ Util.*, 2017, **18**, 89.
10 M. Lashgari and P. Zeinalkhani, *Appl. Catal., A*, 2017, **529**, 91.
11 J. Fu, K. Jiang, X. Qiu, J. Yu and M. Liu, *Mater. Today*, 2020, **32**, 222.
12 X. Li, J. Yu, M. Jaroniec and X. Chen, *Chem. Rev.*, 2019, **119**, 3962.
13 X. Feng, J. I. Cerdá and M. Salmeron, *J. Phys. Chem. Lett.*, 2015, **6**, 1780.
14 X. Shao, X. Yin and J. Wang, *J. Colloid Interface Sci.*, 2018, **512**, 466.
15 M. I. Malik, Z. O. Malaibari, M. Atieh and B. Abussaud, *Chem. Eng. Sci.*, 2016, **152**, 468.
16 M. M. Kandy, *Sustainable Energy Fuels*, 2020, DOI: 10.1039/C9SE00827F.
17 M. Lashgari and P. Zeinalkhani, *Nano Energy*, 2018, **48**, 361.
18 J. Li, F. Meng, S. Suri, W. Ding, F. Huang and N. Wu, *Chem. Commun.*, 2012, **48**, 8213.
19 S. Jana, A. Mondal and A. Ghosh, *Appl. Catal., B*, 2018, **232**, 26.
20 J. Wang, H. Liu, Y. Xu and X. Zhang, *Asian J. Chem.*, 2014, **26**, 3875.
21 X. Du, J. Wei, J. Zhao, R. Han and Y. Ding, *Chem.–Asian J.*, 2014, **9**, 2745.
22 H. Bemana and S. Rashid-Nadimi, *Surf. Interfaces*, 2019, **14**, 184.
23 Y. Jiao, Y. Liu, B. Yin, S. Zhang, F. Qu and X. Wu, *Nano Energy*, 2014, **10**, 90.
24 C. Wang, X. Cheng, X. Zhou, P. Sun, X. Hu, K. Shimanoe, G. Lu and N. Yamazoe, *ACS Appl. Mater. Interfaces*, 2014, **6**, 12031.
25 X. Zhang, C. Wang, H. Li, X. G. Wang, Y. N. Chen, Z. Xie and Z. Zhou, *J. Mater. Chem. A*, 2018, **6**, 2792.
26 S. M. Bashir, S. S. Hossain, S. Rahman, S. Ahmed and M. M. Hossain, *Electrocatalysis*, 2015, **6**, 544.
27 M. Lashgari and M. Ghanimati, *Chem. Eng. J.*, 2019, **358**, 153.
28 M. A. Asi, L. Zhu, C. He, V. K. Sharma, D. Shu, S. Li, J. Yang and Y. Xiong, *Catal. Today*, 2013, **216**, 268.
29 C. B. Andersen, *J. Geosci. Educ.*, 2002, **50**, 389.
30 J. G. Shim, D. W. Lee, J. H. Lee and N. S. Kwak, *Environ. Eng. Res.*, 2016, **21**, 297.
31 M. Lashgari and M. Ghanimati, *J. Photonics Energy*, 2014, **4**, 044099.
32 M. Lashgari and M. Ghanimati, *J. Colloid Interface Sci.*, 2019, **555**, 187.
33 J. Hong, W. Zhang, J. Ren and R. Xu, *Anal. Methods*, 2013, **5**, 1086.
34 R. Gusain, P. Kumar, O. P. Sharma, S. L. Jain and O. P. Khatri, *Appl. Catal., B*, 2016, **181**, 352.
35 Y. Wang, S. Fan, F. Liao, X. Zheng, Z. Huang, Y. Wang and X. Han, *Nanoscale Adv.*, 2019, **1**, 1200.
36 M. Lashgari and M. Ghanimati, *J. Hazard. Mater.*, 2018, **345**, 10.
37 M. Lashgari, P. Elyas-Haghighi and M. Takeguchi, *Sol. Energy Mater. Sol. Cells*, 2017, **165**, 9.
38 M. Lashgari and D. Matloubi, *J. Chem. Sci.*, 2015, **127**, 575.
39 Z. Sun, N. Talreja, H. Tao, J. Texter, M. Muhler, J. Strunk and J. Chen, *Angew. Chem., Int. Ed.*, 2018, **57**, 7610.
40 X. M. Liu, G. Q. Lu, Z. F. Yan and J. Beltramini, *Ind. Eng. Chem. Res.*, 2003, **42**, 6518.
41 N. M. Dimitrijevic, B. K. Vijayan, O. G. Poluektov, T. Rajh, K. A. Gray, H. He and P. Zapol, *J. Am. Chem. Soc.*, 2011, **133**, 3964.
42 J. Wambach, A. Baiker and A. Wokaun, *Phys. Chem. Chem. Phys.*, 1999, **1**, 5071.
43 H. Yamashita, A. Shiga, S. Kawasaki, Y. Ichihashi, S. Ehara and M. Anpo, *Energy Convers. Manage.*, 1995, **36**, 617.
44 Y. Jia, Y. Xu, R. Nie, F. Chen, Z. Zhu, J. Wang and H. Jing, *J. Mater. Chem. A*, 2017, **5**, 5495.

 